Detection of HI 21 cm Power Spectrum: Sensitivity estimates of various Radio Telescopes

Pallav Chanda[1] *
Project Supervisor: Dr. Abhirup Datta[2] †
Working with: Madhurima Choudhury[3] ‡

[1]B.S.M.S., IISER Bhopal.
[2]Associate Professor, IIT Indore.
[3]PhD Research Scholar - DST INSPIRE, IIT Indore.

Host Institute:
Indian Institute of Technology, Indore
(IIT Indore)

Project Period: 10 May 2019 - 7 July 2019

*email: pallav16@iiserb.ac.in
†email: abhirup.datta@iiti.ac.in
‡email: phd1601121002@iiti.ac.in

Abstract

A number of Radio Telescopes and corresponding experiments aim to detect the HI 21 cm Power Spectrum. The detection depends on precise calibration for removing bright foregrounds, and the Sensitivity of the Radio Telescope to the 21 cm Power Spectrum. This work aims to design a code for calculating the Sensitivity of the Murchison Widefield Array (MWA) (both compact and long baseline), and Square Kilometer Array (SKA) Radio Telescopes at redshifts $z \sim 10$ and to get Sensitivity estimates for the aforementioned telescopes along with HERA. 21cmSense package for HERA has been used as a base and further modified for the above listed Radio Telescopes. A detailed derivation of the response of an interferometer to the HI 21 cm Power Spectrum, from two different formalisms which slightly differ from each other, is presented. Further, exploring the effect each formalism has on the Sensitivity estimates for the Radio Telescopes indicates that one formalism showed lesser effects of Sample Variance on the Sensitivity estimates than the other. Few checks have also been performed to ensure Fourier transforms do not introduce abnormalities in the Power Spectrums; and to ensure that adding Signal and Noise in the Image Plane and then calculating Power Spectrum in the k-space is equivalent to adding the Power Spectrums of both Signal and Noise in the k-space which further result into claiming the code to be of robust nature. The UV-coverage from CASA and the code have also been compared. Finally, the Sensitivities of the Radio Telescopes are demonstrated for tracked and drift scans; and discussions about the results obtained follow. SKA is determined to have the highest chance of HI 21 cm Power Spectrum detection and characterization; while HERA and MWA have very low Signal to Noise ratio leading to lower chances of detection.

Contents

1 Introduction

The HI 21 cm Power Spectrum is fascinating to physicists as it speaks a great deal about the evolution of the universe after the Cosmic Dark Ages. The Power Spectrum has within it hidden information about the Epoch of Reionization, galaxy formation and evolution, etc. Using this, we can probe into the conditions that lead to the formation of the universe as we see it today. But detection of this power spectrum at high redshifts still remains a challenge because of the Sensitivities of the Radio Telescopic Arrays of this generation to the signal is quite less.

This work is aimed at developing a robust code for calculating the Sensitivity of a few Radio Telescopes to the 21 cm Power Spectrum, and to get an estimate of the Noise Power Spectrum at various k-modes and compare which Radio Telescope has the least Noise due to the Interferometric response to the Signal. McQuinn et al. [2006] and Parsons et al. [2012] have previously pursued this and have meticulously derived the all the formulae that are needed. Morales [2005] has explored the detector noise covariance-matrices on which the derivation in McQuinn et al. [2006] relies. The derivations proposed in this work follow the same procedure used by both of the aforementioned works with slight modifications for modelling and coding wherever needed. Pober et al. [2013, 2014] also focuses on Sensitivity estimates for BAOBAB and HERA, respectively. This work considers the python package **21cmSense** (click here)[1] for HERA (written by Pober based on his aforementioned works) as a base for further development; for including other Radio Telescopes; and performs a few Validation checks to make sure the code is robust.

Parsons et al. [2012] makes an Array configuration study in which he has predicted a few arrays that will have higher Sensitivity than the others. The next generation of arrays coming up will provide much better tools and sensitivity to detect the HI 21 cm Power Spectrum.

2 The cosmological 21 cm Signal

Hydrogen, being the most abundant atomic species in the universe, can withhold a lot of information about the local properties of the gas. Delving into quantum properties of Hydrogen, the hyperfine splitting causes splitting of the 1S ground state – due to the interaction of the magnetic moments of the proton and the electron – into two distinct energy levels, called the singlet and triplet states, separated by $\Delta E = 5.9 \times 10^{-6}$eV. The wavelength

[1] https://github.com/jpober/21cmSense

corresponding to this ΔE is 21.1 cm and the frequency is 1420 MHz, been measured from studies of hydrogen masers to great accuracy. [Pritchard and Loeb, 2012] A transition of the electron in HI species from one state to the other leads to an emission/absorption of 21 cm wavelength radiation accompanied by a spin flip. Even though the probability of the corresponding transition being one in a billion years, the fact that Hydrogen is the most abundant atomic species leads to the abundant 21 cm signal that is the founding element for 21 cm cosmology.

The 21 cm line is a useful probe for gas along the line of sight to some background radio source in cosmological contexts. However, the observability of the 21 cm signal depends upon the radiative transfer through gas along the line of sight. [Pritchard and Loeb, 2012]

The observed brightness temperature of the 21 cm line at a given frequency ν is given by: [Pritchard and Loeb, 2012]

$$T_b^{obs} = T_{ex}(1 - e^{-\tau_\nu}) + T_R(\nu)e^{-\tau_\nu}, \tag{1}$$

where, T_R is the brightness temperature of a background radio source; T_{ex} is the uniform excitation temperature. The excitation temperature corresponding to the 21 cm line is T_S, called the spin temperature. Spin temperature is mainly determined by 3 main processes: [Pritchard and Loeb, 2012]
(i) The radio background, primarily CMB, absorbing/emitting the 21 cm photons.
(ii) collisions with electrons and with other hydrogen atoms.
(iii) resonant scattering of Lyα photons which lead to a spin flip via an intermediate excited state.

The equilibrium balance of these processes determine the spin temperature and is given by: [Field, 1958]

$$T_S^{-1} = \frac{T_\gamma^{-1} + x_\alpha T_\alpha^{-1} + x_c T_K^{-1}}{1 + x_\alpha + x_c}, \tag{2}$$

where, T_γ is the temperature of the surrounding bath of radio photons, $T_\gamma = T_{CMB}$; T_α is the color temperature of the Lyα radiation field at the Lyα frequency; T_K is the kinetic gas temperature. T_α and T_K are closely coupled by recoil during repeated scattering; x_α, x_c are coefficients of coupling due to scattering of the Lyα photons and atomic collisions, respectively, and, are given by *Wouthuysen-Field effect* [Wouthuysen, 1952, Field, 1958] and *Collisional Coupling effects* [Field, 1958, Furlanetto et al., 2006], respectively.

For using the 21 cm line as a probe of astrophysics, two types of background radio sources are important, each of which have their own benefits of being used. [Pritchard and Loeb, 2012]

(i) CMB can be used as a background radio source in which case, $T_R = T_{CMB}$ and the 21 cm feature, at appropriate radio frequencies, becomes spectral distortion to the CMB blackbody.
(ii) A radio loud point source, such as a radio loud quasar, can be used as the background radio source. Thus, the gas is seen in absorption against the source as the source will always be much brighter than the weak emission from diffuse hydrogen gas, $T_R \gg T_S$.

The 21 cm brightness temperature depends on the volume-averaged ionized fraction of hydrogen which leads to the signal giving a measure of the amount of neutral hydrogen (HI) and ionized hydrogen (HII) being present in the universe at a given point of time. Thus, studying the redshifted 21 cm signal gives information about the evolution of the universe after the Cosmic Dark Ages and about ionization zones/bubbles at high redshifts which have high probabilities for galaxy formation. The redshifted 21 cm signal is also considered to be a unique probe of the conditions during the EoR.

Measurements of the absolute temperature as a function of frequency, averaged over the sky, could help in measuring the global 21 cm signal. Although, the need to remove galactic foregrounds which are much larger than the signal pose a challenge for the signal extraction. For the detection of this highly redshifted 21 cm signal from the EoR, the first generation of experiments have been designed in the last few years. The Low Frequency Array (LOFAR) [Rottgering et al., 2006], the Murchison Widefield Array (MWA) [Lonsdale et al., 2009] and the Donald C. Backer Precision Array for Probing the Epoch of Reionization (PAPER) [Parsons et al., 2010] have started dedicated measurements for long observation times with the aim of detecting the 21 cm power spectrum. The feasibility of accurately characterizing both foreground emission and instrumental systematics will decide the success or failure of these experiments. Even if these experiments are successful in a positive detection of the power spectrum, the features of the signal will be marginal at best due to the limited collecting area. Next generation of larger 21 cm experiments will be needed for characterization of the power spectrum. [Parsons et al., 2012] Another challenge posed is removal of the Noise introduced by the instrument itself, which is again of higher magnitude than the signal and it depends on the instrument or Array used for the detection.

3 Calculating the Sensitivity to the 21 cm Power Spectrum

Sensitivity to the 21 cm Power Spectrum gives a measure of the Noise Power Spectrum of the instrument or Array used. Two formalisms follow from here.

3.1 Formalism used in derivation by Parsons and Pober

3.1.1 Single-baseline Response

Beginning with the basic definitions for the 3D power spectrum of brightness temperature fluctuations (the statistic which 21 cm efforts aim to measure) and for the visibility (the fundamental observable of an interferometer), with respect to the brightness temperature in a pixel of the sky plane/frequency data cube, $T(\vec{x})$, and its Fourier dual $\tilde{T}(\vec{k})$, the convention yields: [Parsons et al., 2012]

$$\begin{aligned}\tilde{T}(\vec{k}) =& \frac{1}{\mathbb{V}} \int T(\vec{x}) e^{-i\vec{k}\cdot\vec{x}} d^3x \\ \tilde{T}(\vec{x}) =& \frac{\mathbb{V}}{(2\pi)^3} \int T(\vec{k}) e^{i\vec{k}\cdot\vec{x}} d^3k.\end{aligned} \tag{3}$$

Here, $\mathbb{V}$ denotes the volume of the observed data cube and $\vec{x}$ is a 3D vector that indicates direction on the sky and depth (the frequency dimension) within the field. $\vec{k}$ is a 3D wave-vector with projection $k_\perp \equiv (k_x, k_y)$ in the plane of the sky, and k_z along the line-of-sight (frequency) direction. Deriving the response in the flat-sky approximation, lets one take $\vec{x}$ to be cartesian. It follows from this convention that an estimate of the power spectrum is given by: [Parsons et al., 2012]

$$\hat{P}(\vec{k}) \equiv \left\langle |\tilde{T}(\vec{k})|^2 \right\rangle = \int \hat{\xi}(\vec{r}) e^{-i\vec{k}\cdot\vec{r}} d^3r, \tag{4}$$

where, angle brackets refer to an ensemble average, $\vec{r}$ is the vector distance between two points, and $\hat{\xi}(\vec{r})$ is an estimate of the two-point correlation function of the measured T , given by [Parsons et al., 2012]

$$\hat{\xi}(\vec{r}) = \frac{1}{\mathbb{V}} \int T(\vec{x}) T(\vec{x} + \vec{r}) d^3x. \tag{5}$$

Equation (2-21) in Thompson [1999] defines visibility as: [Thompson,

1999]

$$V(u,v,w,\nu) \equiv \int \frac{dl\ dm}{\sqrt{1-l^2-m^2}} A(l,m,\nu) I(l,m,\nu) \times e^{-2\pi i(ul+vm+w(\sqrt{1-l^2-m^2}-1))}, \tag{6}$$

where, $l \equiv \sin\theta_x$ and $m \equiv \sin\theta_y$ are (in the small-angle approximation) angular coordinates in image domain, ν is spectral frequency, $A(l,m,\nu)$ is a windowing function describing the field-of-view and bandpass response of an interferometer pair, $I(l,m,\nu)$ is the specific intensity, $(u,v,w) \equiv \vec{b}/\lambda$ are the east-west, north-south, and line-of-sight projections of baseline vector $\vec{b}$ toward a phase center, in units of observing wavelength λ.

Extending the definition of the visibility in the flat-sky approximation [Clark, 1999] leads to inclusion of a Fourier transform along the frequency axis: [Parsons et al., 2012]

$$\tilde{V}(u,v,\eta) \approx \int dl\ dm\ d\nu\ A(l,m,\nu) I(l,m,\nu) \times e^{-2\pi i(ul+vm+\eta\nu)}. \tag{7}$$

This definition ignores the frequency-dependence of (u,v) arising from the changing length of λ dividing the physical separation of two antennas.

Squaring both sides and using $I = 2k_B T/\lambda^2$, with λ being the mean wavelength over the sub-band used in the Fourier transform, yields [Parsons et al., 2012]

$$\tilde{V}^2(u,v,\eta) \approx \left(\frac{2k_B}{\lambda^2}\right)^2 \int dl\ dm\ d\nu\ dl'\ dm'\ d\nu' \times A(l,m,\nu) T(l,m,\nu) A(l',m',\nu') T(l',m',\nu') \times e^{-2\pi i[u(l-l')+v(m-m')+\eta(\nu-\nu')]}. \tag{8}$$

Now, making the approximation that $A(l,m,\nu)$ is a top-hat windowing function and explicitly integrating $A(l,m,\nu)$ determines the width and shape of the convolution kernel in Equation (13). Since the width of this kernel is thereafter neglected and only enters later to tally the number of independent wave-modes sampled, the top-hat approximation should be considered purely pedagogical. Drawing $A(l,m,\nu)$ into the bounds of the integral yields: [Parsons et al., 2012]

$$\tilde{V}^2(u,v,\eta) \approx \left(\frac{2k_B}{\lambda^2}\right)^2 \int_{(0,0,0)}^{(\theta,\theta,B)} dl dm d\nu \int_{(0,0,0)}^{(\theta,\theta,B)} dl' dm' d\nu' \times T(l,m,\nu) T(l',m',\nu') \times e^{-2\pi i[u(l-l')+v(m-m')+\eta(\nu-\nu')]}, \tag{9}$$

where, $\theta \equiv \Omega$, for primary beam field-of-view Ω. Changing variables so that $(l_r, m_r, \nu_r) = (l - l', m - m', \nu - \nu')$: [Parsons et al., 2012]

$$\begin{aligned}\tilde{V}^2(u,v,\eta) \approx \left(\frac{2k_B}{\lambda^2}\right)^2 [&\int_{(-\theta,-\theta,-B)}^{(0,0,0)} dl_r dm_r d\nu_r \\ &\times \int_{(0,0,0)}^{(\theta+l_r,\theta+m_r,B+\nu_r)} dl dm d\nu \\ &+ \int_{(0,0,0)}^{(\theta,\theta,B)} dl_r dm_r d\nu_r \\ &\times \int_{(l_r,m_r,\nu_r)}^{(\theta,\theta,B)} dl dm d\nu] \\ &\times T(l,m,\nu) T(l-l_r, m-m_r, \nu-\nu_r) \\ &\times e^{-2\pi i(ul_r + vm_r + \eta\nu_r)}.\end{aligned} \tag{10}$$

Integrating over (l, m, ν) and using Equation (5) yields:

$$\begin{aligned}\tilde{V}_{21}^2(u,v,\eta) \approx \left(\frac{2k_B}{\lambda^2}\right)^2 \Omega B &\int_{(-\theta,-\theta,-B)}^{(\theta,\theta,B)} dl_r dm_r d\nu_r \\ &\times \hat{\xi_{21}}(l_r, m_r, \nu_r) e^{-2\pi i(ul_r + vm_r + \eta\nu_r)},\end{aligned} \tag{11}$$

where, B is the observing bandwidth, and where the subscript "21" is now used to make explicit that these quantities are derived for emission from reionization. Using X and Y to represent conversion factors from angle and frequency to comoving distance, respectively, leads to the substitution $(Xl_r, Xm_r, Y\nu_r)$ for (r_x, r_y, r_z) and (Xk_x, Xk_y, Yk_z) for $2\pi(u, v, \eta)$. The factor of 2π follows from the cosmological Fourier convention. This substitution then yields [Parsons et al., 2012]

$$\tilde{V}_{21}^2(u,v,\eta) \approx \left(\frac{2k_B}{\lambda^2}\right)^2 \frac{\Omega B}{X^2 Y} \int_{-X\theta,-X\theta,-YB}^{X\theta,X\theta,YB} \hat{\xi_{21}}(\vec{r}) e^{-i\vec{k}\cdot\vec{r}} d^3r, \tag{12}$$

This equation establishes the relationship between a (u, v, η)-mode measured by an interferometer and a $\vec{k}$-mode. Hereafter "(u, v, η)-mode" and "$\vec{k}$-mode" have been used interchangeably to refer to a coherent region in Fourier space. Because the right-hand side of Equation (12) is the Fourier transform of $\xi(\vec{r})$ with a top-hat window, in Fourier space it becomes the convolution of the Fourier transform of these functions: [Parsons et al., 2012]

$$\begin{aligned}\tilde{V}_{21}^2(u,v,\eta) \approx \left(\frac{2k_B}{\lambda^2}\right)^2 \frac{\Omega B}{X^2 Y} &[\hat{P}_{21}(\vec{k}) * (sinc(2X\theta k_x) \\ &\times sinc(2X\theta k_y) sinc(2YBk_z))],\end{aligned} \tag{13}$$

where, '$*$' signifies convolution in $\vec{k}$. In the more general case this convolving kernel is not a sinc function, but the Fourier transform of the primary beam $\tilde{A}(l, m, \nu)$. For primary beam responses larger than 30 arcmin, the width of the kernel in k-space is much smaller than the scales over which $P_{21}(\vec{k})$ varies for the k-modes that are likely not to be dominated by foregrounds [McQuinn et al., 2006]. Thus, we drop the sinc kernel from Equation (13), giving: [Parsons et al., 2012]

$$\tilde{V}_{21}^2(u, v, \eta) \approx \left(\frac{2k_B}{\lambda^2}\right)^2 \frac{\Omega B}{X^2 Y} \hat{P}_{21}(\vec{k}). \tag{14}$$

Expressing the 21 cm signal in a dimensionless manner given by $\hat{\Delta}^2(k) \equiv \frac{k^3}{2\pi^2}\hat{P}(\vec{k})$ (using that $\hat{P}_{21}(\vec{k})$ is expected to be nearly isotropic; McQuinn et al. [2006]), Equation (14) can be written as

$$\tilde{V}_{21}^2(u, v, \eta) \approx \left(\frac{2k_B}{\lambda^2}\right)^2 \frac{\Omega B}{X^2 Y} \frac{2\pi^2}{k^3} \hat{\Delta}_{21}^2(k). \tag{15}$$

3.1.2 Single-Baseline Sensitivity Measuring One $\vec{k}$-mode

Calculating the power spectrum of the thermal noise of an instrument is the next step for estimating the sensitivity to the 21 cm signal. Thermal fluctuations produce a white-noise signal with root-mean-square (RMS) brightness temperature $T_{N,rms}$, which is mostly equivalent to the sky temperature for 21 cm instruments. The thermal noise contributes a component to the RMS amplitude of the visibility $\tilde{V}_N$ equal to: [Parsons et al., 2012]

$$\tilde{V}_N = \frac{2k_B}{\lambda^2} T_{N,rms} \Omega B. \tag{16}$$

By assuming a white-spectrum thermal noise for I with temperature $T_{N,rms}$ in Equation (6), Equation (16) can be arrived at. Substituting $\tilde{V}_N$ for $\tilde{V}$ in Equation (15) to get the noise contribution to the dimensionless power, $\Delta_N^2(k)$, yielding [Parsons et al., 2012]

$$\Delta_N^2(k) \approx X^2 Y \frac{k^3}{2\pi^2} \Omega B T_{N,rms}^2(u, v, \eta). \tag{17}$$

There are $2Bt$ independent measurements of the noise for time t. The value of $T_{N,rms}$ in Equation (17) is the error in how well T_{sys} can be measured – which depends on the error in how well thermal noise can be measured

and subtracted off) – and for Gaussian random noise is $\sqrt{2}T_{sys}$ or $T^2_{N,rms} = T^2_{sys}/Bt$. Thus, [Parsons et al., 2012]

$$\Delta^2_N(k) \approx X^2 Y \frac{k^3}{2\pi^2}\frac{\Omega}{2t}T^2_{sys}, \tag{18}$$

where, t is the integration time for sampling a particular (u, v, η)-mode, and the factor of two in the denominator comes from the explicit inclusion of two orthogonal polarizations to measure the total unpolarized signal. Thus, the power-spectrum sensitivity for a k-mode is independent of band-width. Also, [Furlanetto et al., 2006]

$$X \approx 1.9 \left(\frac{1+z}{10}\right)^{0.2} h^{-1} \ \frac{\text{Mpc}}{\text{arcmin}}, \tag{19}$$

$$Y \approx 17 \left(\frac{1+z}{10}\right)^{\frac{1}{2}} \left(\frac{\Omega_m h^2}{0.15}\right)^{-\frac{1}{2}} \ \frac{\text{Mpc}}{\text{MHz}}, \tag{20}$$

which gives (for $\Omega_m = 0.27$):

$$X^2 Y \approx 540 \left(\frac{1+z}{10}\right)^{0.9} \ \frac{h^{-3}\ \text{Mpc}^3}{\text{sr} \cdot \text{Hz}}. \tag{21}$$

3.1.3 Combining Independent k-mode Measurements

Now that the sensitivity of one baseline to one k-mode has been derived, the focus shifts to the sensitivity boost that comes from combining multiple baselines. Combining statistically independent k-modes improves the sensitivity proportionally to the square root of the number of samples, $N_s^{1/2}$.

Pober's code, **21cmSense** [Pober et al., 2013, 2014], uses only the sensitivity boost that comes from combining *multiple time samples* in a sidereal day, which in turn depends on the number of time bins available for measuring $\Delta^2_{21}(k)$ Such additional samples grow linearly with the daily observation length, $t_{\text{per\_day}}$ (Combination of samples over multiple days has already been accomplished in Equation (18).) Thus, the sensitivity increases as [Parsons et al., 2012]

$$\Delta^2_N(k) \propto \left[\frac{1}{t_{\text{per\_day}}}\right]^{\frac{1}{2}} \Delta^2_{N,0}(k). \tag{22}$$

3.1.4 Sample Variance

Redundant samples of various modes have been used to beat down thermal noise. Hence, simply counting Fourier modes over an effective survey volume

will not give an estimate of the sample variance. Since the ratio of thermal noise to sample variance can vary between every measured k-mode, a weighted combination of these modes must be taken in order to create a 1-D or 2-D power spectrum out of the full 3-D Fourier space. Combining each measurement at a particular k-mode using inverse-variance, one finds that the optimal estimator of the power spectrum results in an error that can be calculated by combining the errors on each measured mode in inverse-quadrature: [Pober et al., 2013]

$$\delta\Delta^2(k) = \left(\sum_i \frac{1}{\left(\Delta^2_{N,i}(k) + \Delta^2_{21}(k)\right)^2} \right)^{-\frac{1}{2}}, \tag{23}$$

where, $\delta\Delta^2(k)$ is the resultant uncertainty on a given k-mode, $\Delta^2_{N,i}$ is the per-mode thermal noise calculated with Equation (18) taking the full uv-coverage and earth-rotation synthesis into account, $\Delta^2_{21}(k)$ is the cosmological 21 cm power spectrum (which is also the sample variance error), and i is an index labeling the independent k-modes measured by the array over which we are summing.

3.2 Formalism used in derivation by McQuinn

The visibility for a pair of antennae, quantified as temperature, is given by [McQuinn et al., 2006]

$$V(u, v, \nu) = \int d\hat{\boldsymbol{n}}\ \Delta T_b(\hat{\boldsymbol{n}}, \nu) A_\nu(\hat{\boldsymbol{n}}) e^{2\pi i \binom{u}{v}\cdot\hat{\boldsymbol{n}}}, \tag{24}$$

where, (u, v) is a vector that gives the number of wavelengths at frequency ν between the antennae and $A_\nu(\hat{\boldsymbol{n}})$ is the contribution to the primary beam in the direction $\hat{\boldsymbol{n}}$. We have assumed flat sky approximation. [Clark, 1999]

Assuming that the visibilities are complex Gaussian random variables, such that the likelihood function of the covariance matrix $C_{ij} = \langle V_i^*\ V_j \rangle$ for n visibilities, where the asterisk indicates a complex conjugate, is [McQuinn et al., 2006]

$$\mathcal{L}(C) = \frac{1}{\pi^n \det C}\ \exp\left[-\sum_{i,j}^{n}\ V_i^*\ C_{ij}^{-1}\ V_j \right]. \tag{25}$$

When counting the number of independent $u - v$ pixels one should restrict to the half space because the visibilities are complex and $V(u, v, \nu) = V(-u, -v, -\nu)^*$. C will be dominated by the detector noise on most scales.

The RMS detector noise fluctuation per visibility of an antennae pair after observing for a time t_0 in one frequency channel is [Rohlfs and Wilson, 2004]

$$\Delta V^N = \frac{\lambda^2 T_{sys}}{A_e \sqrt{\Delta\nu \; t_0}} \tag{26}$$

where, $T_{sys}(\nu)$ is the total system temperature, A_e is the effective area of an antenna, and $\Delta\nu$ is the width of the frequency channel.

For an observation with bandwidth B, where $B \gg \Delta\nu$, if the observed visibilities are Fourier transformed in the frequency direction, a 3-D map of $\tilde{I}(\boldsymbol{u}) \equiv \int d\nu \; V(u,v,\nu)\exp\left[2\pi i\nu\eta\right]$, in which $\boldsymbol{u} = u\hat{\boldsymbol{i}} + v\hat{\boldsymbol{j}} + \eta\hat{\boldsymbol{k}}$ and η has dimensions of time is obtained. If this transform is performed on just the detector noise component $\boldsymbol{V}^N$ of the visibility map $\boldsymbol{V}$, one has [McQuinn et al., 2006]

$$\tilde{I}^N(\boldsymbol{u}) = \sum_{i=1}^{B/\Delta\nu} V^N(u,v,\nu_i)\exp\left[2\pi i\nu_i\eta\right]\Delta\nu \tag{27}$$

$$\tilde{I}^N(\boldsymbol{u}) = \sum_{i=1}^{B/\Delta\nu} V'^N(u,v,\nu_i)\Delta\nu, \tag{28}$$

where, $\exp\left[2\pi i\nu\eta\right]$ has been absorbed into a new variable V'^N that has the same RMS as V^N and the frequency channels $\nu_1, ..., \nu_{B/\Delta\nu}$ are spaced $\Delta\nu$ apart. It follows that the detector noise covariance matrix for a single baseline is [Morales, 2005]

$$\begin{aligned} C^N_{1b}(\boldsymbol{u}_i,\boldsymbol{u}_j) &= \left\langle \tilde{I}^N(\boldsymbol{u}_i)^* \; \tilde{I}^N(\boldsymbol{u}_j) \right\rangle \\ &= \left\langle \left(\sum_{m=1}^{B/\Delta\nu} V'^N(\boldsymbol{u}_i,\nu_m)\Delta\nu \right)^* \right. \\ &\quad \left. \times \left(\sum_{l=1}^{B/\Delta\nu} V'^N(\boldsymbol{u}_j,\nu_l)\Delta\nu \right) \right\rangle \end{aligned}$$

$$C^N_{1b}(\boldsymbol{u}_i,\boldsymbol{u}_j) = B \; \Delta\nu \left(\Delta V^N\right)^2 \delta_{ij} \tag{29}$$

$$C^N_{1b}(\boldsymbol{u}_i,\boldsymbol{u}_j) = \left(\frac{\lambda^2 B T_{\rm sys}}{A_e}\right)^2 \frac{\delta_{ij}}{B t_0}. \tag{30}$$

To reach Equation (29), note that different $V'^N(\boldsymbol{u}_i,\nu_m)$ are uncorrelated, and Equation (30) follows from Equations (26) and (29). Note that Equation (30)

only depends on B and not on $\Delta\nu$: finer frequency resolution comes at no added cost.

By estimating the average observing time $t_{\boldsymbol{k}}$ for an array of antennae to observe a mode $\boldsymbol{k}$ as follows: [McQuinn et al., 2006]

$$t_{\boldsymbol{k}} \approx \frac{A_e t_0}{\lambda^2}\, n\left(x|\boldsymbol{k}|\sin\theta/2\pi\right), \tag{31}$$

where, t_0 is the total observing time for the interferometer, θ is defined to be the angle between k and the LOS, and $n(\cdot)$ denotes number density. Thus, the detector noise covariance matrix for an interferometer can be written as: [McQuinn et al., 2006]

$$C^N(\boldsymbol{k}_i, \boldsymbol{k}_j) = \left(\frac{\lambda^2 B T_{\rm sys}}{A_e}\right)^2 \frac{\delta_{ij}}{B t_{\boldsymbol{k}_i}}. \tag{32}$$

(From this point onwards, $\boldsymbol{k}$ is used to index elements in C rather than $\boldsymbol{u}$).

An expression for the contribution to C owing to sample variance is also needed. For a 3-D window function $W(\hat{\boldsymbol{n}}, \nu) = A_\nu(\hat{\boldsymbol{n}}) F_{\hat{\boldsymbol{n}}}(\nu)$, assuming that different pixels indexed by $\boldsymbol{u}$ are uncorrelated, the covariance matrix of the 21 cm signal $\tilde{I}^{21}$ can be written as: [McQuinn et al., 2006]

$$\begin{aligned} C^{SV}(\boldsymbol{k}_i, \boldsymbol{k}_j) &= \left\langle \tilde{I}^{21}(\boldsymbol{u}_i)^* \tilde{I}^{21}(\boldsymbol{u}_j) \right\rangle \\ &\approx \delta_{ij} \int d^3\boldsymbol{u}' |\tilde{W}(\boldsymbol{u}_i - \boldsymbol{u}')|^2 P^{21}_{\Delta T}(\boldsymbol{u}'), \end{aligned} \tag{33}$$

where, $\langle \Delta T^{21}(\boldsymbol{u}') \Delta T^{21}(\boldsymbol{u}) \rangle = P_{\Delta T}(\boldsymbol{u}) \delta^3(\boldsymbol{u}' - \boldsymbol{u})$ and the definition of visibility from Equation (24) has been used. One can simplify C^{SV} further: [McQuinn et al., 2006]

$$C^{SV}(\boldsymbol{k}_i, \boldsymbol{k}_j) \approx P^{21}_{\Delta T}(\boldsymbol{u}_i) \frac{\lambda^2 B}{A_e} \delta_{ij} \tag{34}$$

$$C^{SV}(\boldsymbol{k}_i, \boldsymbol{k}_j) \approx P^{21}_{\Delta T}(\boldsymbol{k}_i) \frac{\lambda^2 B^2}{A_e X^2 Y} \delta_{ij}, \tag{35}$$

where, X and Y hold the same meaning as in Section 3.1.1 according to Parsons' and Pober's formalism. Further details about the above simplification can be looked up in McQuinn et al. [2006] Section 3.

A large number of independent Fourier cells will be observed in a region of real space volume, Vol $= X^2 Y \lambda^2 / A_e$, over the course of an observation. The 21 cm power spectrum is symmetric around the polar angle ϕ. Hence, all the Fourier cells in an annulus of constant (k, θ) with radial width Δk

and angular width $\Delta\theta$ are summed for a statistical detection. The number of independent cells in such an annulus is [McQuinn et al., 2006]

$$N_c(k,\theta) = 2\pi k^2 \sin\theta \Delta k \Delta\theta \times \frac{\text{Vol}}{(2\pi)^3}. \tag{36}$$

Here, $(2\pi)^3/\text{Vol}$ is the resolution in Fourier space. However, binning as (k,θ) comes with its own set of problems. One would rather prefer to bin as $(k, k_\parallel)$, where $k_\parallel = \sqrt{k_x^2 + k_y^2}$. This sort of binning helps because the size of both k-bin and $k_\parallel$-bin are defined by the Bandwidth (B), number of channels (nchan) and the channel width ($\Delta\nu$) which can be defined by the user in Pober's **21cmSense**. [Pober et al., 2013, 2014] (Note that, the following derivation is being done for the purpose of correctly calculating the sensitivity boost obtained from combination of various independent k-modes and it does not necessarily exist in McQuinn et al. [2006] formalism.) From the definition of θ,

$$\begin{aligned} \theta &= \arccos\frac{k_\parallel}{k} \\ \implies \frac{\Delta\theta}{\Delta k_\parallel} &= \frac{1}{\sqrt{1-\left(\frac{k_\parallel}{k}\right)^2}} \times \frac{1}{k} \\ \implies \frac{\Delta\theta}{\Delta k_\parallel} &= \frac{k}{k_\perp} \times \frac{1}{k} \end{aligned}$$

Substituting the value of $\Delta\theta$ from above and also that $\sin\theta = \frac{k_\perp}{k}$ (note that, $k_\perp$ and k_z are one and the same thing and can be used interchangably) into Equation (36) we obtain:

$$N_c(k,k_\parallel) = 2\pi k \Delta k \Delta k_\parallel \times \frac{\text{Vol}}{(2\pi)^3}. \tag{37}$$

For the calculations, Equation (37) is used for N_c when the wavelength corresponding to $\boldsymbol{k}$ fits within the survey volume (i.e. when $2\pi/k_\parallel < Y$ and otherwise $N_c = 0$.

Equations (32) and (35) are summed to get C, the error in $P_{\Delta T}^{21}(\boldsymbol{k})$ from a measurement in a bin with $N_c(k,k_\parallel)$ pixels is [McQuinn et al., 2006]

$$\delta P_{\Delta T}^{21}(k,k_\parallel) \approx \sqrt{\frac{1}{N_c}} \frac{A_e X^2 Y}{\lambda^2 B^2} \left[C^{SV}(k,k_\parallel) + C^N(k,k_\parallel)\right], \tag{38}$$

where, $C(\boldsymbol{k}) \equiv C(\boldsymbol{k},\boldsymbol{k})$ is defined. Expressing in terms of Dimensionless Power Spectrum $\hat{\Delta}^2(k) \equiv \frac{k^3}{2\pi^2}\hat{P}(\vec{k})$, one has:

$$\delta\Delta_{21}^2(k,k_\parallel) \approx \sqrt{\frac{1}{N_c}} \frac{k^3}{2\pi^2} \frac{A_e X^2 Y}{\lambda^2 B^2} \left[C^{SV}(k,k_\parallel) + C^N(k,k_\parallel)\right]. \tag{39}$$

Since, even here, *multiple time samples* in a sidereal day are being combined, the sensitivity boost arising from that also needs to be considered. Section 3.1.3 describes the same which can be used here without any need for modifications. Equation (22) gives the sensitivity boost as: [Parsons et al., 2012]

$$\Delta^2_N(k) \propto \left[\frac{1}{t_{\text{per\_day}}}\right]^{\frac{1}{2}} \Delta^2_{N,0}(k).$$

4 Studying the 21cmSense Code for HERA

21cmSense [Pober et al., 2013, 2014] is a python package for calculating the expected sensitivity of HERA to the power spectrum of the 21 cm Signal at the Epoch of Reionization. **21cmSense** package was downloaded from its GitHub page [2] and installed by following instructions in the `README` file. The package contains two main scripts: `mk_array_file.py` and `calc_sense.py` . The inputs to `mk_array_file.py` are also python scripts called calibration files which cannot be executed independently. The inputs to `calc_sense.py` are the array files generated by `mk_array_file.py`

4.1 Calibration files

Calibration files include all the information about the array one is trying to calculate the sensitivities for including the positions of all the antennas in the array, the antenna size, system temperature, etc. The calibration file included in **21cmSense** is for HERA.

4.2 `mk_array_file.py`

This script generates an array file containing the UV-coverage of the specific antenna array. It needs calibration file as input and returns a `.npz` file containing the UV-coverage of the array (both when all baselines within a uv pixel are added coherently and when non-instantaneously redundant baselines are added incoherently), observation duration, dish size in units of wavelength, temperature of the receiver, integration time per visibility, and the central frequency of the observation.

usage: `python mk_array_file.py -C [calfile] [options]`

[2] https://github.com/jpober/21cmSense

The script provides options like `--track, --bl_min, --bl_max, --freq` which the user can use to set the duration of a tracked scan in hours, minimum and maximum baselines in meters to be included in the UV-plane and the central frequency of the observation, respectively. The central frequency of the observation determines the redshift of our observation corresponding to the 21 cm line. Default values are specified for each option in case the user decides to specify no options. In case the option `--track` is not specified, the script assumes a drift scan. Accordingly, the array file is produced.

4.3 `calc_sense.py`

This script calculates sensitivity of an array to the 21 cm Signal. It is the main portion of the package. The formula used in the code is the one derived in Section 3.1 according to the derivation by Parsons and Pober. It needs array file generated by `mk_array_file.py` as input and returns a `.npz` file containing the k-values, Sensitivity (Thermal Noise Only), and Full Sensitivity (Thermal Noise and Sample Variance).

usage: `python calc_sense.py [options] [*array_file_name].npz`

The script provides options like `--model, --buff, --eor, --ndays, --n_per_day, --bwidth, --nchan, --no_ns` which the user can use to set the model of the foreground wedge to use (three options are pess (pessimistic), mod (moderate) and opt (optimistic)), the size of the additive buffer outside the horizon to exclude in the pessimistic and moderate models, the model epoch of reionization power spectrum, the total number of days observed, the number of good observing hours per day, cosmological bandwidth in GHz, number of channels across cosmological bandwidth, and remove pure north/south baselines, respectively. Default values are specified for each option in case the user decides to specify no options. The model epoch of reionization power spectrum can be an output from 21cmFAST. A redshift 9.5 $\sim$50% ionization model produced by 21cmFAST has been included in the package as the default model epoch of reionization power spectrum to use. The default sensitivity is calculated for 180 days of observation (`--ndays`) for both drift and tracked scans with 6 hours of good observing hours per day (`--n_per_day`). For a tracked scan, number of good observing hours per day should be an integer multiple of the tracked duration. This leads to a default total observation duration of $180 \times 6 = 1080$ hours.

5 Validating the Codes

To check if the Fourier transforms stated in Section 3.1.1 work correctly and do not introduce any unknown or unrelated features in the Power Spectrum, and to understand if adding Noise Power Spectrum to the 21 cm Signal Power Spectrum in the k-space was equivalent to adding Noise with 21 cm HI map (from which the Power Spectrums were obtained) in the image plane first and then evaluating the Power Spectrum.

For this, a GRF (Gaussian Random Field) with $\mu = 0$ and $\sigma = \frac{T_{\rm sys}}{\sqrt{\Delta\nu\ \Delta t}}$, where, $\Delta\nu$ is the channel width and Δt is the integration time per visibility, has been generated for simulating Noise in the Image Plane. We call this as the 'Noise'. Further its Power Spectrum has been calculated in the k-space.

A simulation of the 21 cm HI map has been obtained from a seminumerical code (which was again in the Image Plane). We call this as the 'Signal'. Further its Power Spectrum has been calculated in the k-space.

Both the Power Spectrums of 'Signal' and 'Noise' have been added in the k-space.

Also, the 'Noise' and the 'Signal' have been added in the Image Plane, pixel to pixel. We call this as 'Signal + Noise'. The corresponding Power Spectrum of 'Signal + Noise' has been calculated in the k-space.

Further, the calculated Power Spectrum of the 'Signal' has been compared with other Power Spectrums of 21 cm Signal from **21cmFAST**.

Codes have been written for all the above stated calculations and simulations.

Also, in order to check that the UV-coverage output by `mk_array_file.py` is correct, we generate a UV-map for VLA (Very Large Array) Radio Telescope with track duration 1 min and integration time per visibility as 10 sec for a point source at the phase centre using CASA. This was compared with the UV-coverage of VLA generated using `mk_array_file.py` for the same parameters.

6 Sensitivity to the 21 cm Signal for other Radio Telescopes

6.1 Calibration files for other Radio Telescopes

The other Radio Telescopes we have considered here include MWA (compact), MWA (long baseline) and SKA. Calibration files need to be made for other arrays so that `mk_array_file.py` can use the calibration file to generate UV-coverage for those Radio Telescopes. For this, most of the mod-

ifications are restricted to the `ARRAY SPECIFIC PARAMETERS` section of the calibration file. A list of antenna positions of a Radio Telescope is saved in `[*array_name]_antpos.csv` file. In the Calibration file,
(i) `antpos` is an array of (x, y, z) coordinates taken as input from the `[*array_name_antpos].csv` file.
(ii) `loc` specifies the (Lat, Long) location of the Centre of the Antenna Array of the Radio Telescope.
(iii) `dish_size_in_lambda` specifies the Dish Size of an antenna of the Radio Telescope and converts it in units of wavelength. The conversion has been elaborated for better user interpretation.
(iv) `Trx` is the temperature of the receiver (later used in `calc_sense.py` to calculate T_{sys}) but need not be used here (and hence can be left unchanged without any impact) as we are further going to consider a slightly different model for computing the system temperature T_{sys} for the Radio Telescopes. Other parameters need not be changed as they are perfectly scaled by modifying the above parameters.

Outside of `ARRAY SPECIFIC PARAMETERS` section, modifications have also been made in the FWHM calculation of the beam in order to make it easier for user interpretation and slightly more accurate. Further the calculation of observation duration for a drift scan has also been modified in order to make it easier for user interpretation with added comments. A following table lists the Array Specific Parameters that have been used for the calibration files for those Radio Telescopes.

Radio Telescope	Number of antennae	Latitude, Longitude (of Centre)	Dish Size (in m)
HERA	127	(38:25:59.24, -79:51:02.1)	14.0
MWA (compact)	128	(-26:42:11.95, 116:40:14.93)	4.0
MWA (long baseline)	128	(-26:42:11.95, 116:40:14.93)	4.0
SKA	512	(-26:49:29.18, 116:45:51.84)	40.0

Table 1: Array Specific Parameters

6.2 Modifications to `mk_array_file.py`

Pober's code for `mk_array_file.py` requires `numpy v1.2.0` to work. Higher `numpy` versions give error when trying to run it. Since, `numpy v1.2.0` is now

a legacy version, few changes have been made throughout the code in order to make it compatible with the latest `numpy` version (`v1.15.4`).
Further, a small bug in the code in line `85`:

```
uvbin = '%.1f,%.1f' % (u,v)
```

leads to `(u, v)` values near 0 (i.e. 0^- and 0^+) sometimes creating different `uvbin`s due to the presence of the $-$ sign for 0^- values while rounding off and consequently retaining the sign while being stored as a string in `uvbin`. This leads to extra `uvbin`s being created at rare occasions. Modifying that code piece as:

```
if round(u,1) == 0.0:  u = 0.0
if round(v,1) == 0.0:  v = 0.0
uvbin = '%.1f,%.1f' % (u,v)
```

fixes the bug and accurately finds the number of redundant baselines.

For Radio Telescopes with a large number of antennas and correspondingly large number of baselines or very long baselines (e.g. MWA (long baseline), SKA), the `mk_array_file.py` can take days or even weeks to get the UV-coverage. Thus, in case the user has higher has higher memory and higher processing power available, one can decide to trade off memory for speed. For this reason, a new script has been written named `fast_mk_array_file.py` which implements 3-D arrays for storing data and also a few function definitions so as to speed up the code by as much as 10-12% while consuming 4-6 times the memory consumed by `mk_array_file.py` for that particular Radio Telescopes. The user can choose to use it depending on machine configuration. The code will give a memory error in case the code does not have sufficient space to run on a particular machine.

6.3 Modifications to `calc_sense.py`

The model of system temperature we have used for other Radio Telescopes is different from the one used in `calc_sense.py` for HERA. We use,

$$T_{\rm sys}(\nu) = 180 \text{ K} \left(\frac{\nu}{180 \text{ MHz}}\right)^{-2.5} \tag{40}$$

where, K denotes Kelvin units and ν is the Central frequency of the observation (which determines the observing redshift) in MHz units. Hence, necessary modifications have been made in the code `calc_sense.py` . No changes have been made to the default values of the options.

6.4 Implementing McQuinn's formalism

21cmSense uses the formalism and formulae described in Section 3.1 for estimating the Sensitivity of an array to the 21 cm Signal. However, we have

implemented the formalism and formulae stated in McQuinn et al (2008) described in Section 3.2 in a new script named `calc_sense_mcquinn.py`. The motivation behind this exercise is to observe what effect it has on the sensitivity estimates and determine which one gives a better estimate. It has been made sure that all the functionality of `calc_sense.py` has been carried forward to `calc_sense_mcquinn.py`, and hence, the default values of all the options remain the same.

7 Results

7.1 Validation Checks

The Check performed as stated in Section 5 shows that: The Power Spectrum of 'Signal' added with the Power Spectrum of 'Noise' is almost similar to the Power Spectrum of 'Signal + Noise'.

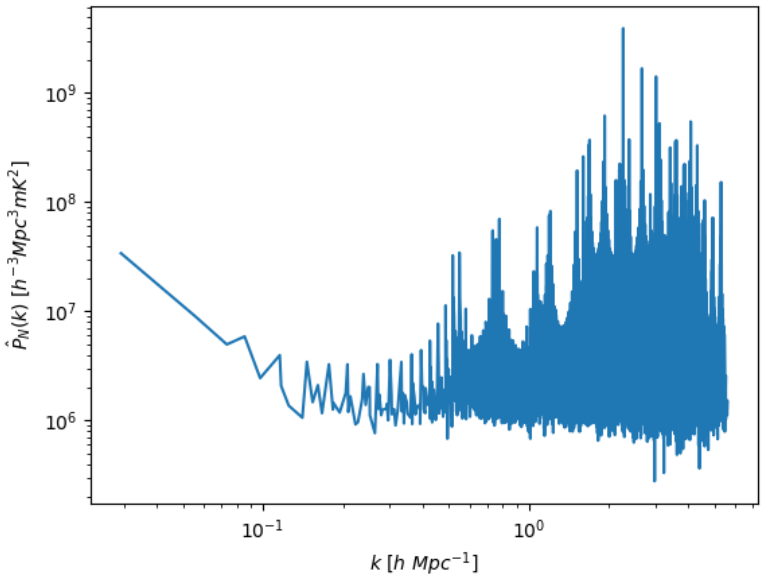

Figure 1: Noise Power Spectrum (unbinned) $\hat{P}_N(k)$

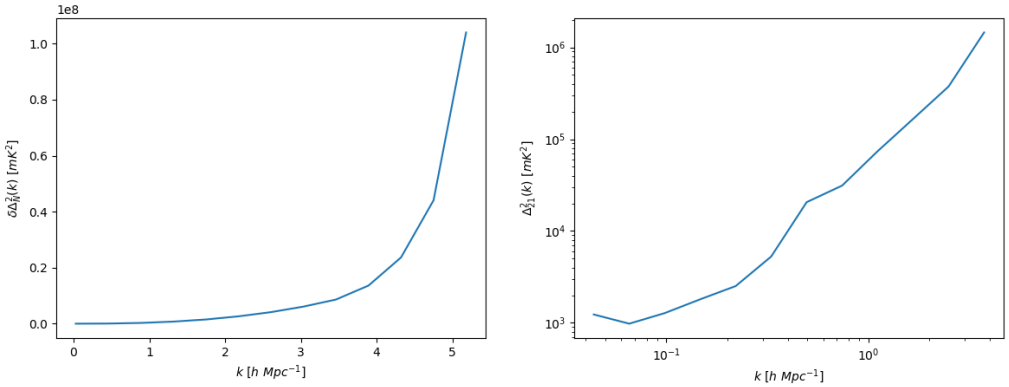

(a) Noise Power Spectrum $\Delta^2_N(k)$ (b) Signal Power Spectrum $\Delta^2_{21}(k)$

Figure 2: Power Spectrums

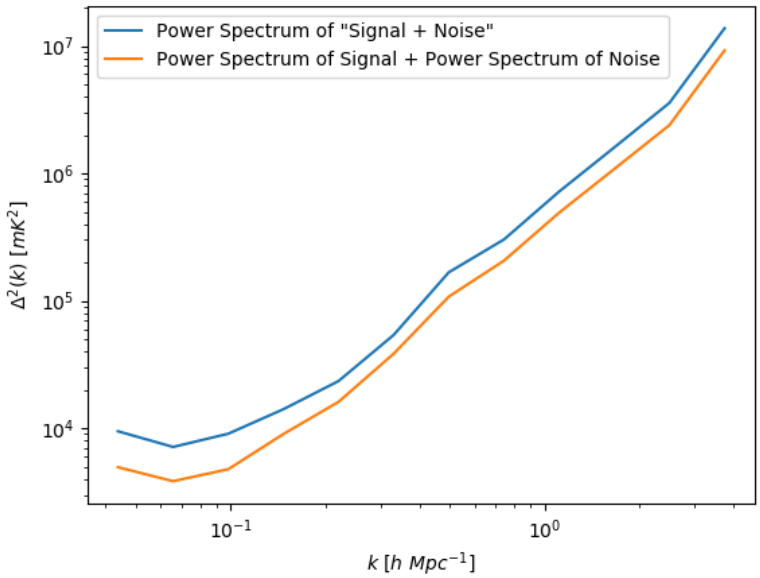

Figure 3: Validation Check

Also, the UV-map generated for VLA using the stated parameters in Section 5 from CASA is almost similar to the UV-coverage given by `mk_array_file.py` .

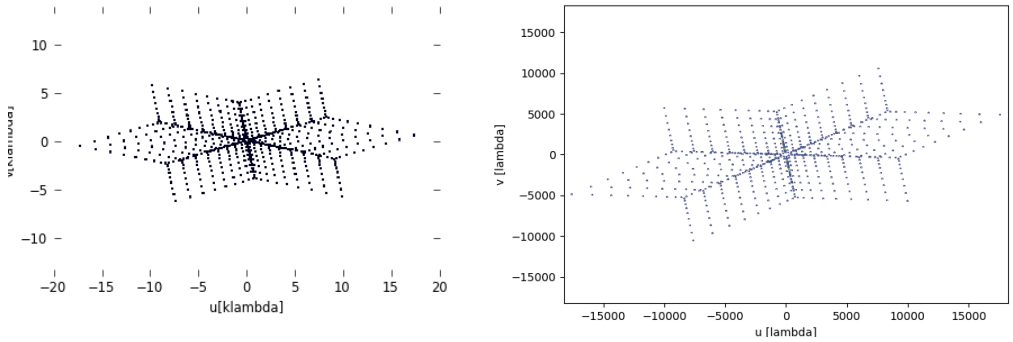

(a) From CASA (b) From `mk_array_file.py`

Figure 4: UV-Coverage of VLA for 1min comparison

7.2 UV-coverage and Sensitivity Estimates

UV-Coverage plots and Sensitivity plots have been obtained for the Radio Telescopes by using the calibration files that were written for them, and by using `calc_sense.py` with the new model for system temperature described in Equation 40. A table below lists the simulation model parameters like duration of a track scan, maximum baseline included, etc. used, for which the plots have been obtained.

Radio Telescope	Scan Type	Track Duration (in a day)	Maximum baseline present	Maximum baseline included
HERA	Drift	-	168 m.	168 m.
	Track	6 hr.	168 m.	168 m.
MWA (compact)	Drift	-	740.79 m.	740.79 m.
	Track	6 hr.	740.79 m.	740.79 m.
MWA (long baseline)	Drift	-	5302.87 m.	1000 m.
	Track	6 hr.	5302.87 m.	600 m.
SKA	Drift	-	64671.92 m.	10000 m.
	Track	6 hr.	64671.92 m.	5000 m.

Table 2: Simulation Model Parameters

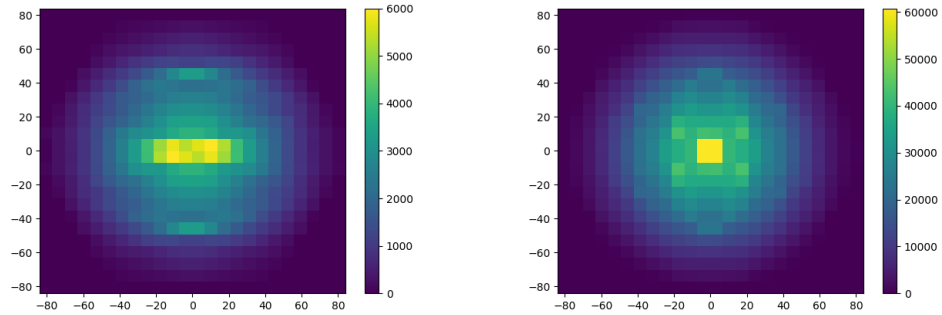

(a) Drift (b) Track 6hr

Figure 5: HERA UV Coverage

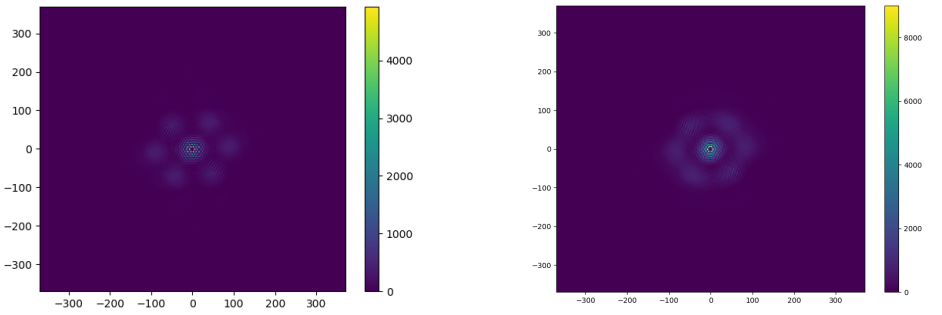

(a) Drift (b) Track 6hr

Figure 6: MWA compact UV Coverage

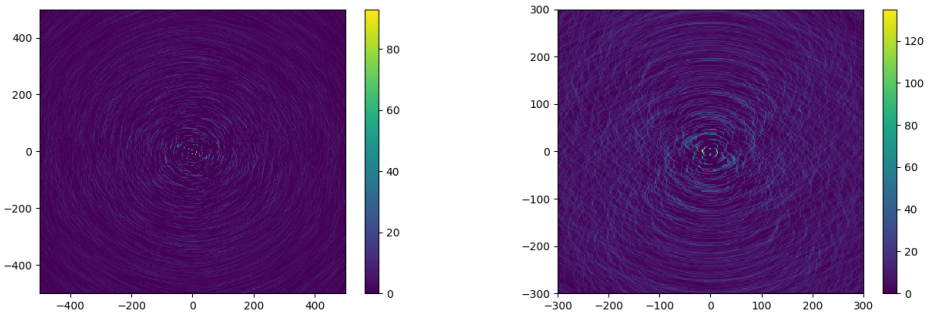

(a) Drift (b) Track 6hr

Figure 7: MWA long baseline UV Coverage

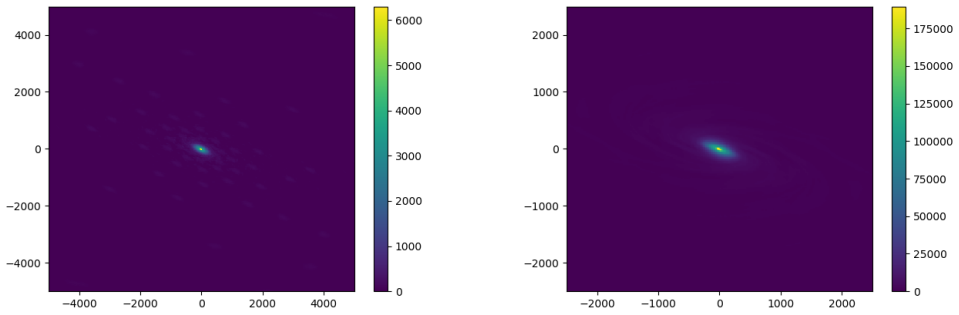

(a) Drift (b) Track 6hr

Figure 8: SKA UV Coverage

The Sensitivity estimates calculated with default values for all the options have been plotted for a few configurations. (For all the calculated Sensitivities, Total observing time = 1080 hours)

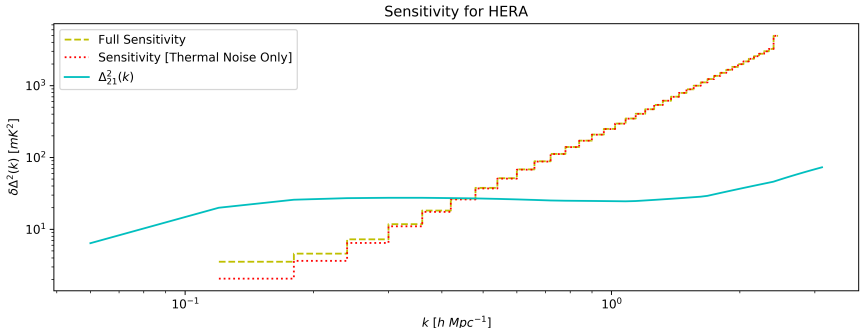

(a) Drift

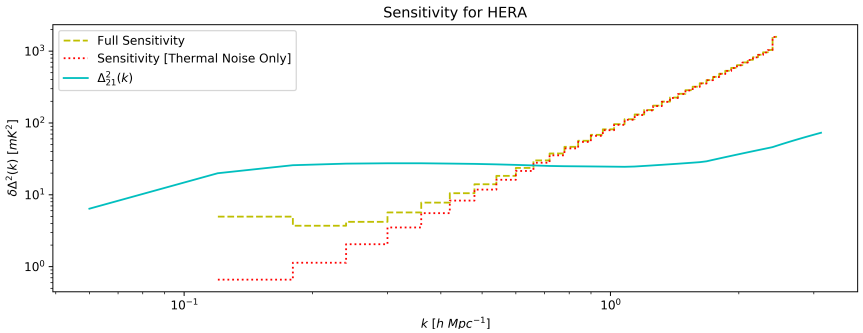

(b) Track 6hr

Figure 9: Sensitivities for HERA

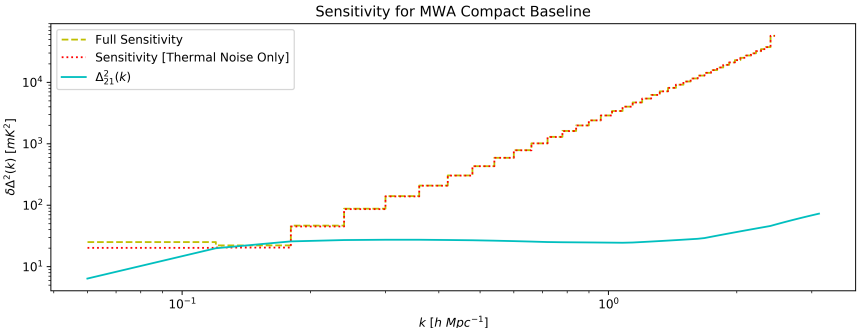

(a) Drift

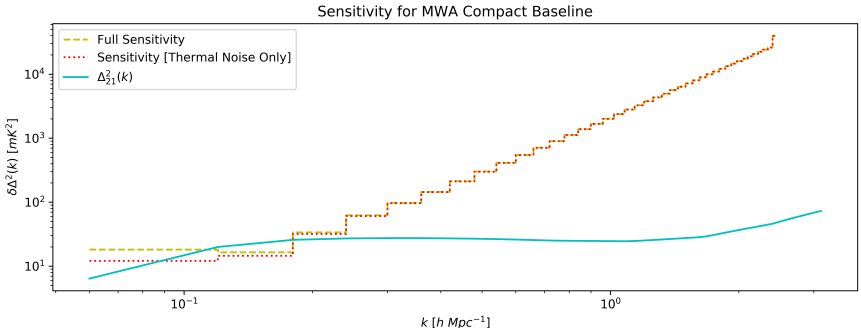

(b) Track 6hr

Figure 10: Sensitivities for MWA compact

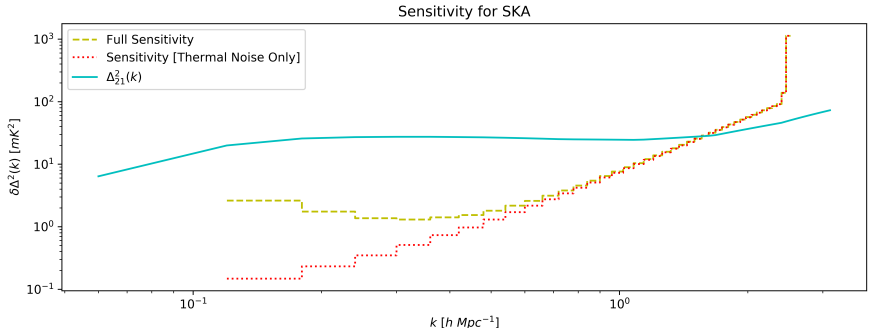

(a) Drift

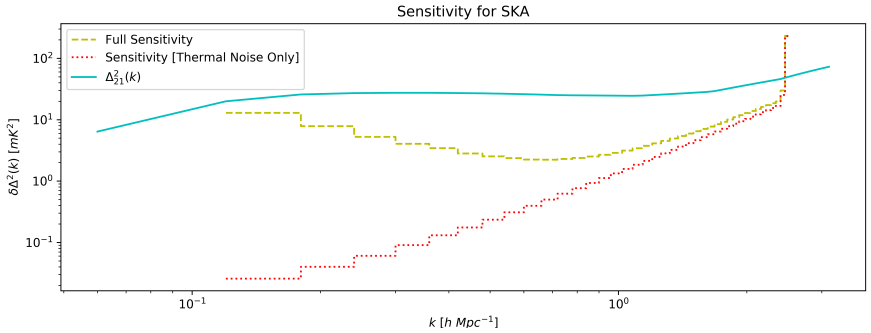

(b) Track 6hr

Figure 11: Sensitivities for SKA

8 Conclusions

From the validation checks (see Figure 3), it has been concluded that adding Noise Power Spectrum to the 21 cm Signal Power Spectrum in the k-space was equivalent to adding Noise with 21 cm HI map (from which the Power Spectrums were obtained) in the Image Plane first and then evaluating the Power Spectrum; and that the Fourier transforms are not introducing any unrelated features in the Signal. The comparison of 1 min UV-coverages of VLA (Figures 4a 4b) show that the UV-coverage obtained from both CASA and `mk_array_file.py` are almost similar with a slight phase difference in the one from `mk_array_file.py` . This can attributed to some phase difference introduced by the source object which is not being created exactly at the zenith of phase centre.

It has also been concluded that the UV-coverages obtained from both `mk_array_file.py` and `fast_mk_array_file.py` are exactly the same, and have been tested by using multiple simulation model parameters, while the

latter being 10-12% faster each single time. Memory error was not obtained on any occasion, though that mostly depends on the machine specifications used to run the code. Hence, `fast_mk_array_file.py` can be used without any issues for all our future needs.

Comparing the Sensitivity Estimates obtained from `calc_sense.py` and `calc_sense_mcquinn.py`, it has been realised that the sensitivity estimates from both are almost similar within statistical error limits. However, `calc_sense_mcquinn.py` gives very low changes in sensitivity after including sample variance which indicates `calc_sense_mcquinn.py` using McQuinn's formalism (Section 3.2) gives better Sensitivity Estimates. At lower k-modes, Full Sensitivity Estimates using `calc_sense.py` show a higher effect of Sample Variance.

Sensitivity Estimates show much lower Noise values for a Tracked scan than a Drift Scan. Also, the Noise values can be lowered further by increasing the total observation duration.

Sensitivity Estimates for all the Radio Telescopes show a trend of having lower Noise values at lower k-modes and higher Noise values (much higher than the 21 cm Signal itself) at higher k-modes. This indicates that we have a much higher chance of HI 21cm Signal detection at lower k-modes during observations if only Thermal Noise from the Telescope is taken into account. However, this is not the realistic scenario. Galactic Foregrounds have a much higher power spectrum (of the order of 10^6 times the Signal), and have a trend of higher values at lower k-modes and lower values at higher k-modes. Hence, the realistic statistical 21 cm Signal detection would depend on the statistics of both the Sensitivity of the Radio Telescope and the Foregrounds. Although, since Galactic Foregrunds have a overall smooth Power Spectrum, the Signal detection will likely be possible for data from Radio Telescopic arrays which have Noise values lower than the Signal for most of the k-modes into consideration. Comparing the Sensitivity Estimates for all the Radio Telescopes we have considered, we conclude that SKA has the lowest Noise Power Spectrum and has the highest possibility of a HI 21 cm Signal detection.

Next generation of Radio Telescopes will bring higher chance of 21 cm Signal detection even at moderate k-modes with very low Noise values and also the power to characterize the 21 cm Power Spectrum. 21 cm Cosmology has a bright future to look forward to in the upcoming years.

Acknowledgements

First and foremost, I would like to thank Dr. Abhirup Datta for giving me the opportunity to work on this project which I have dearly come to love and developed a keen interest in. His guidance has been valuable throughout and his insights have, at many places, made me more evaluative. This project would also not have been possible without the help of Ms. Madhurima Choudhury, who has played the role of a Co-Guide, has always been upfront for any clarifications in understanding of both theory and code, and is a very inquisitive person. A heartfelt thanks to her would still be less for her help.

I would also like to thank Mr. Arnab Chakraborty, PHD Scholar working with Dr. Abhirup Datta, for his deep insights into UV-space, and Visibility theory – without him, understanding of a few things would not have been possible. A special thanks to Ms. Aishrila Mazumder, PHD Scholar working with Dr. Abhirup Datta, for her extensive help in providing whatever simulations were needed from her at the soonest possible.

A big thank you to IIT, Indore for hosting me for a duration of 2 months, and to DAASE, IIT Indore for allowing me to use BAZINGA, their HPC machine. Last but not the least, I would like to thank SHE, INSPIRE Fellowship for funding this project; and IISER, Bhopal – my dear college – for sorting out any issues regarding the funding and for allowing me to pursue this project.

References

Matthew McQuinn, Oliver Zahn, Matias Zaldarriaga, Lars Hernquist, and Steven R. Furlanetto. Cosmological Parameter Estimation Using 21 cm Radiation from the Epoch of Reionization. , 653(2):815–834, Dec 2006. doi: 10.1086/505167.

Aaron Parsons, Jonathan Pober, Matthew McQuinn, Daniel Jacobs, and James Aguirre. A Sensitivity and Array-configuration Study for Measuring the Power Spectrum of 21 cm Emission from Reionization. , 753(1):81, Jul 2012. doi: 10.1088/0004-637X/753/1/81.

Miguel F. Morales. Power Spectrum Sensitivity and the Design of Epoch of Reionization Observatories. , 619(2):678–683, Feb 2005. doi: 10.1086/426730.

Jonathan C. Pober, Aaron R. Parsons, David R. DeBoer, Patrick McDonald, Matthew McQuinn, James E. Aguirre, Zaki Ali, Richard F. Bradley, Tzu-Ching Chang, and Miguel F. Morales. The Baryon Acoustic Oscillation Broadband and Broad-beam Array: Design Overview and Sensitivity Forecasts. , 145(3):65, Mar 2013. doi: 10.1088/0004-6256/145/3/65.

Jonathan C. Pober, Adrian Liu, Joshua S. Dillon, James E. Aguirre, Judd D. Bowman, Richard F. Bradley, Chris L. Carilli, David R. DeBoer, Jacqueline N. Hewitt, and Daniel C. Jacobs. What Next-generation 21 cm Power Spectrum Measurements can Teach us About the Epoch of Reionization. , 782(2):66, Feb 2014. doi: 10.1088/0004-637X/782/2/66.

Jonathan R. Pritchard and Abraham Loeb. 21 cm cosmology in the 21st century. *Reports on Progress in Physics*, 75(8):086901, Aug 2012. doi: 10.1088/0034-4885/75/8/086901.

George B. Field. Excitation of the Hydrogen 21-CM Line. *Proceedings of the IRE*, 46:240–250, Jan 1958. doi: 10.1109/JRPROC.1958.286741.

S. A. Wouthuysen. On the excitation mechanism of the 21-cm (radio-frequency) interstellar hydrogen emission line. , 57:31–32, Jan 1952. doi: 10.1086/106661.

Steven R. Furlanetto, S. Peng Oh, and Frank H. Briggs. Cosmology at low frequencies: The 21 cm transition and the high-redshift Universe. , 433 (4-6):181–301, Oct 2006. doi: 10.1016/j.physrep.2006.08.002.

H. J. A. Rottgering, R. Braun, P. D. Barthel, M. P. van Haarlem, G. K. Miley, R. Morganti, I. Snellen, H. Falcke, A. G. de Bruyn, and R. B. Stappers. LOFAR - Opening up a new window on the Universe. *arXiv e-prints*, art. astro-ph/0610596, Oct 2006.

C. J. Lonsdale, R. J. Cappallo, M. F. Morales, F. H. Briggs, L. Benkevitch, J. D. Bowman, J. D. Bunton, S. Burns, B. E. Corey, and L. Desouza. The Murchison Widefield Array: Design Overview. *IEEE Proceedings*, 97(8): 1497–1506, Aug 2009. doi: 10.1109/JPROC.2009.2017564.

Aaron R. Parsons, Donald C. Backer, Griffin S. Foster, Melvyn C. H. Wright, Richard F. Bradley, Nicole E. Gugliucci, Chaitali R. Parashare, Erin E. Benoit, James E. Aguirre, and Daniel C. Jacobs. The Precision Array for Probing the Epoch of Re-ionization: Eight Station Results. , 139(4): 1468–1480, Apr 2010. doi: 10.1088/0004-6256/139/4/1468.

A. Richard Thompson. Fundamentals of Radio Interferometry. In G. B. Taylor, C. L. Carilli, and R. A. Perley, editors, *Synthesis Imaging in Radio Astronomy II*, volume 180 of *Astronomical Society of the Pacific Conference Series*, page 11, Jan 1999.

B. G. Clark. Coherence in Radio Astronomy. In G. B. Taylor, C. L. Carilli, and R. A. Perley, editors, *Synthesis Imaging in Radio Astronomy II*, volume 180 of *Astronomical Society of the Pacific Conference Series*, page 1, Jan 1999.

Kristen Rohlfs and Thomas L. Wilson. *Tools of radio astronomy*. 2004.